ces (see appendix D) is clearly seen, together with the mirror symmetries between the two enantiomers. Importantly, these symmetries also imply that for unpolarized light, and in complete consistency with Fig. 1, the total intensity transmitted by the structures is independent of the chosen enantiomer. Furthermore, the conversion of polarization is well (geometrically) illustrated by using the Poincaré sphere representation [25]. Indeed, as shown in Fig. 3, the Mueller matrix defines a geometrical transformation which projects the unit Poincaré sphere, drawn by the input Stokes vector, on an output closed surface with typical radius $F\left(\mathcal{M}^{\text{exp.}}\right) \simeq 1$ in agreement with the absence of net depolarization as already noticed (from theory, $F\left(\mathcal{M}^{\text{th.}}\right) = 1$ exactly). Data shown on Fig. 2 are also plotted on this sphere. The input state draws a circle in the equator plane while the output state (for each enantiomer) draws a circle in a different plane, which center is not located at the center of the sphere. This is a direct manifestation of planar chirality (see appendix E). There is clearly an antisymmetrical behaviour between both enantiomers. The good agreement

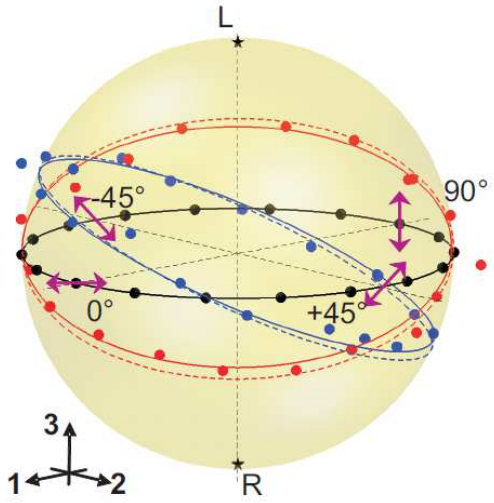

FIG. 3: Full polarization tomography. Poincaré sphere of unit radius associated with the input state represented by the Stokes vector $\mathbf{X}$ [3, 25]. Also shown are the results of Fig. 2 for the left (blue) and right handed (red) structures if the linearly polarized incident state draw the black circle in the (X_1, X_2) equator plane of the input sphere. Data points are compared with the predictions from ${\mathcal{M}_{\mathcal{L},\mathcal{R}}}^{\text{exp.}}$ (continuous curves) and of equation (2) (dashed curves).

between the experiment and the prediction of equations (1,2) shows the sensitivity of the polarization tomography method and the high reliability of the FIB fabrication.